Synthesis, molecular structure investigations and antimicrobial activity of 2-thioxothiazolidin-4-one derivatives

ARTICLE *in* JOURNAL OF MOLECULAR STRUCTURE · FEBRUARY 2015

Impact Factor: 1.6 · DOI: 10.1016/j.molstruc.2014.10.038

8 AUTHORS, INCLUDING:

Abdullah Al Majid
King Saud University
81 PUBLICATIONS **321** CITATIONS
SEE PROFILE

Yahia Mabkhot
King Saud University
86 PUBLICATIONS **337** CITATIONS
SEE PROFILE

Mohamed Al-agamy
King Saud University, College of Pharmacy,...
38 PUBLICATIONS **247** CITATIONS
SEE PROFILE

Hazem A. Ghabbour
King Saud University
134 PUBLICATIONS **186** CITATIONS
SEE PROFILE

Journal of Molecular Structure 1081 (2015) 519–529

Contents lists available at ScienceDirect

Journal of Molecular Structure

journal homepage: www.elsevier.com/locate/molstruc

Synthesis, molecular structure investigations and antimicrobial activity of 2-thioxothiazolidin-4-one derivatives

Assem Barakat [a,c,*,1], Hany J. Al-Najjar [a,1], Abdullah Mohammed Al-Majid [a,1], Saied M. Soliman [b,c,1], Yahia Nasser Mabkhot [a,1], Mohamed H.M. Al-Agamy [d,e,1], Hazem A. Ghabbour [f,1], Hoong-Kun Fun [f,g,1]

[a] Department of Chemistry, College of Science, King Saud University, P.O. Box 2455, Riyadh 11451, Saudi Arabia
[b] Department of Chemistry, College of Science & Arts, King Abdulaziz University, P.O. Box 344, Rabigh 21911, Saudi Arabia
[c] Department of Chemistry, Faculty of Science, Alexandria University, P.O. Box 426, Ibrahimia, 21321 Alexandria, Egypt
[d] Microbiology and Immunology Department, Faculty of Pharmacy, Al-Azhar University, Cairo, Egypt
[e] Division of Microbiology, Pharmaceutics Department, College of Pharmacy, King Saud University, P.O. Box 2457, Riyadh 11451, Saudi Arabia
[f] Department of Pharmaceutical Chemistry, College of Pharmacy, King Saud University, P.O. Box 2457, Riyadh 11451, Saudi Arabia
[g] X-ray Crystallography Unit, School of Physics, Universiti Sains Malaysia, Penang 11800, Malaysia

HIGHLIGHTS

- A series of 2-thioxothiazolidin-4-one derivatives have been synthesized.
- The structure for **3** was elucidated by X-ray diffraction.
- MEP, NBO and FMO were studied using DFT calculations.
- *In-vitro* evaluation of antibacterial and antifungal potencies were carried out.

GRAPHICAL ABSTRACT

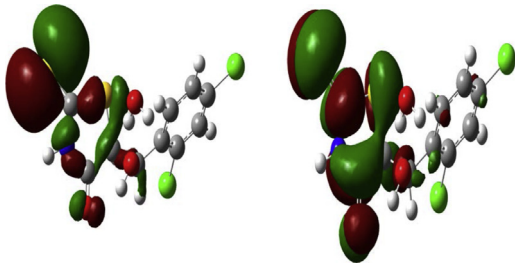

ARTICLE INFO

Article history:
Received 27 August 2014
Received in revised form 24 September 2014
Accepted 16 October 2014
Available online 1 November 2014

Keywords:
Rhodanine
2-Thioxothiazolidin-4-one
Anti-microbial activity
X-Ray
DFT studies

ABSTRACT

A variety of 2-thioxothiazolidin-4-one derivatives were prepared and their *in vitro* antimicrobial activities were studied. Most of these compounds showed significant antibacterial activity specifically against Gram-positive bacteria, among which compounds **4a**,**e**,**g**, **5b**,**e**,**g**,**h** and **6f** exhibit high levels of antimicrobial activity against *Bacillus subtilis* ATCC 10400 with Minimum Inhibitory Concentration (MIC) value of 16 μg/mL. All compounds have antifungal activity against *Candida albicans*. Unfortunately, however, none of the compounds were active against Gram-negative bacteria. The chemical structure of **3** was confirmed by X-ray single crystal diffraction technique. DFT calculations of **3** have been performed on the free $C_{10}H_7Cl_2NO_2S_2$, **3a** and the H-bonded complex, $C_{10}H_7Cl_2NO_2S_2{\cdot}H_2O$, **3b** to explore the effect of the H-bonding interactions on the geometric and electronic properties of the studied systems. A small increase in bond length was observed in the C12–O6 due to the H-bonding interactions between **3a** and water molecule. MEP study has been used to recognize the most reactive sites towards electrophilic and nucleophilic attacks as well as the possible sites for the H-bonding interactions. The TD-DFT calculations have been used to predict theoretically the electronic spectra of the studied compound. The most intense transition band is predicted at 283.9 nm due to the HOMO-2/HOMO-1 to LUMO

* Corresponding author at: Department of Chemistry, College of Science, King Saud University, P.O. Box 2455, Riyadh 11451, Saudi Arabia. Tel.: +966 1467 5884; fax: +966 1467 5992.
E-mail address: ambarakat@ksu.edu.sa (A. Barakat).
[1] These authors contributed equally to this work.

http://dx.doi.org/10.1016/j.molstruc.2014.10.038
0022-2860/

transitions. NBO analyses were carried out to investigate the stabilization energy of the various intramolecular charge transfer interactions within the studied molecules.

Introduction

The treatment of infectious diseases still remains an important and challenging problem. The extensive search of novel antimicrobial agents is a current field of growing interest. Many compounds have been synthesized with this aim but their clinical use has been limited by their relatively high risk of toxicity, ineffectiveness, bacterial resistance and/or pharmacokinetic deficiencies. Infectious diseases are responsible for a significant proportion of deaths worldwide according to WHO. With all of these in mind, there is an urgent need for the discovery or optimization of novel antimicrobial agents that are active against these resistant strains [1]. The diversity in the biological response of 4-thiazolidinones has attracted the attention of many researchers to explore this framework for its potential. The 4-thiazolidinone ring system is a core structure in various synthetic pharmaceuticals displaying a broad spectrum of biological activity, such as antiviral, anti-inflammatory, anticonvulsant, anti-proliferative, anti-diabetic, cardiovascular, anti-tubercular, anti-hyperlipidemic, antibacterial, and antifungal properties. Compounds such as pioglitazone (hypoglycemic), etozoline (antihypertensive), ralitoline (anticonvulsant), and thiazolidomycin (activity against *streptomyces* species), based on this pharmacophore are already in the market (Fig. 1). In recent years, 4-thiazolidinone derivatives with antitumor activity on melanoma, leukemia, colon, lung, ovarian, CNS, renal, breast and prostate cancers cell lines have become a promising area of research. Different researchers have reviewed the progress on the scaffold from time to time, such as Jain et al. [2], Hamama et al. [3], Verma et al. [4], Abdel-Rahman et al. [5], Singh et al. [6], and our group has also been continuously involved in researching this nucleus through chemical modifications with encouraging results [7].

Indeed, 4-thiazolidinones have many interesting activity profiles including non-nucleoside inhibitors of HIV-RT [8], namely COX-1 inhibitors [9], antidiabetic [10], inhibitors of aldose reductase [11,12], inhibitors of the bacterial enzyme MurB which is a precursor acting during the biosynthesis of peptidoglycan and YycG histidine kinase [13,14]. Moreover derivatives of 4-thiazolidinones have been reported for anthelmintic, antitubercular and antifungal activities [2].

Thiazolidinones with C-2 and N-3 substituted positions possess diverse degrees of inhibition against bacteria and fungi. The SAR studies of thiazolidinone derivatives showed that they are more effective on Gram-negative bacteria as compared to Gram-positive bacteria. The search for new antimicrobial agents will continuously remain as an important and challenging task for medicinal chemists. With this in mind and as part of our ongoing studies towards the development of new antimicrobial agents, the various structural modifications in the series of synthesized compounds were evaluated against a variety of pathogens for their antibacterial and antifungal activity. DFT calculations have also been performed to simulate the effect of H-bonding interactions on the molecular structure and electronic properties of the investigated systems. TD-DFT calculations were used to predict the accurate electronic transitions and to draw the HOMO and LUMO levels. The natural bond orbital (NBO) calculations were used to predict the stabilization energies due to intramolecular charge transfer (ICT) within the studied systems.

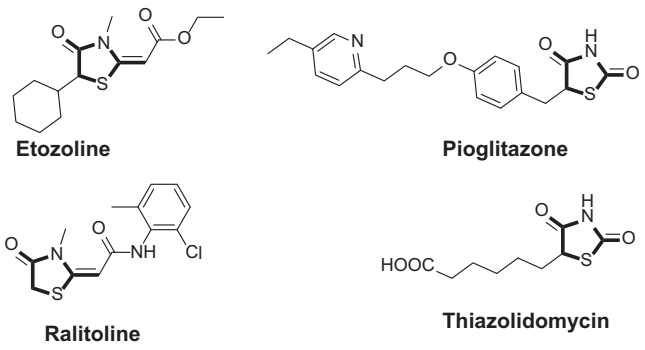

Fig. 1. Some biologically important thiazolidinone compounds.

Experimental

Materials and methods

All the chemicals were purchased from Sigma–Aldrich, Fluka etc., and were used without further purification, unless otherwise stated. Melting point was measured on a Gallenkamp melting point apparatus in open glass capillaries and is uncorrected. IR Spectra were measured as KBr pellets on a Nicolet 6700 FT-IR spectrophotometer. The NMR spectra were recorded on a Jeol-400 NMR spectrometer. ^{1}H NMR (400 MHz), and ^{13}C NMR (100 MHz) were run in deuterated dimethylsulfoxide (DMSO-d_6). Chemical shifts (δ) are referred in terms of ppm and *J*-coupling constants are given in Hz. Mass spectra were recorded on a Jeol of JMS-600 H. Elemental analysis was carried out on Elmer 2400 Elemental Analyzer; CHN mode.

*Synthesis of 5-((2,4-dichlorophenyl)(hydroxy)methyl)-2-thioxothiazolidin-4-one (**3**)*

A mixture of 2,4-dichlorobenzaldehyde (3 mmol, 525 mg), 2-thioxothiazolidin-4-one **1** (3 mmol, 400 mg), and diethylamine (3 mmol, 310 µl) in 3 mL of degassed H_2O was stirred at room temperature for 30 min, the crude product was extracted with mixture of DCM/EtOH, was with 10%HCl (2 × 10 mL), the organic phase was with brine and recrystallized from DCM/EtOH to afford **3** yellow crystalline material (0.8 g, 2.6 mmol, 87%). m.p: 80 °C; IR (KBr, cm^{-1}): 3450, 3015, 1744, 1350; ^{1}H NMR (400 MHz, DMSO-d_6): δ 8.35 (bs, 1H, NH), 7.70(s, 1H, Ph), 7.60–7.25 (m, 4H, CH&CH& Ph); ^{13}C NMR (100 MHz, DMSO-d_6): δ = 198.1, 177.8, 136.1, 134.9, 133.7, 131.6, 129.8, 128.2, 67.1, 65.1; LC/MS (ESI): 309 [M]$^{+}$; Anal. for $C_{10}H_7Cl_2NO_2S_2$; calcd: C, 38.97; H, 2.29; Cl, 23.01; N, 4.54; Found: C, 39.01; H, 2.31; Cl, 23.12; N, 4.57.

Antimicrobial activity

Chemical compounds were individually tested against a panel of gram positive and negative bacterial pathogens. Antimicrobial tests were carried out by the agar well diffusion method [15–17] using 100 mL of suspension containing 1 × 10^{8} CFU/mL of pathological tested bacteria, 1 × 10^{6} CFU/mL of yeast and 1 × 10^{4} spore/mL of fungi spread on nutrient agar (NA), Sabourand dextrose agar (SDA), and potato dextrose agar (PDA) medium respectively. After the media had cooled and solidified, wells (10 mm in diameter)

were made in the solidified agar and loaded with 100 mL of tested compound solution prepared by dissolving 100 mg of the chemical compound in one mL of dimethyl sulfoxide (DMSO). The inculcated plates were then incubated for 24 h at 37 °C for bacteria and 48 h at 28 °C for fungi. Negative controls were prepared using DMSO employed for dissolving the tested compound. Ciprofloxacin (50 mg/mL) and Ketoconazole (50 mg/mL) were used as standard for antibacterial and antifungal activity respectively. After incubation time, antimicrobial activity was evaluated by measuring the zone of inhibition against the test organisms and compared with that of the standard. The observed zone of inhibition is presented in Table 1. Antimicrobial activities were expressed as inhibition diameter zones in millimeters (mm) as follows: N.A. (no activity) $\leqslant$ 4 mm; + (weak) = 5–9 mm; ++ (moderate) = 10–15 mm; +++ (strong) = 16–20 mm and ++++ (very strong) $\geqslant$ 21 mm. The experiment was carried out in triplicate and the average zone of inhibition was calculated.

Determination of MIC for active compounds

MIC of the 19 compounds and two standard controls (ciprofloxacin and itraconazole) were performed by microbroth dilution method as proposed by European Committee on Antimicrobial Susceptibility Testing (EUCAST, 2014). Briefly, the compounds were dissolved in dimethylsulfoxide to give final concentration 1024 mg/mL, and then two fold dilutions were made in the 2× Mueller–Hinton broth (Oxoid Chemical Co. UK) for antibacterial and in 2× RPMI broth for antifungal activity, to give final concentration 512 mg/mL. A 50 μL of broth was dispensed into wells of sterile 96 microtitre plate. A 50 μL of the tested compounds (512 mg/μL) was pipetted into the wells in first well and mixed the contents by using multipippetor by pipetting up and down 6–8 times. Then 50 μL from the first column was withdrawn and added to the second well to make a twofold dilution. This procedure was repeated down to 12th well to reach the concentration of 0.25 μg/mL. A 50 μL was discarding from 12th well. *Staphylococcus aureus* ATCC 29213, *Enterococcus faecalis* ATCC 2912 and *B. subtilis* ATCC 1040 were grown in the tryptone soy broth to the right A560. However *C. albicans* ATCC 2091 was grown in Sabouraud dextrose broth to the right A530. A 100 μL of bacterial inoculums (1×10^5 – 1×10^6 CFU/mL) was dispensed into wells to give final bacterial inocula was 0.5×10^5 – 0.5×10^6 CFU/mL. The microtiter plates were incubated at 35 °C for 18 h. After the incubation period, the results of MIC were recorded manually and interpreted according to the recommendations of EUCAST. MIC is defined as the highest dilution of the drug that kills or inhibits the visible growth of microorganism.

Table 1
Hydrogen bond parameters for **3**.

D–H···*A*	*D*–H	H···*A*	*D*···*A*	*D*–H···*A*
O1WA–H1WA···O2A	0.8200	1.9300	2.738 (2)	168.00
O1WA–H3WA···O1WB	0.8900	1.8100	2.703 (3)	173.00
O1WB–H1WB···O2B	0.8000	1.9800	2.763 (2)	167.00
O1WB–H2WB···O1WA	0.7500	1.9500	2.703 (3)	173.00
N1A–H1NA···O1WB[(i)]	0.82 (3)	2.01 (3)	2.783 (3)	157 (3)
N1B–H1NB···O1WA[(ii)]	0.83 (3)	1.96 (3)	2.755 (3)	160 (3)
O2A–H1OA···O1B[(iii)]	0.84 (3)	1.90 (3)	2.732 (3)	175 (4)
O2B–H1OB···O1A[(iv)]	0.81 (3)	1.97 (3)	2.766 (3)	166 (3)

Symmetry codes:
(i) $-x+2, -y+1, -z+1$.
(ii) $-x+1, -y+1, -z+1$.
(iii) $x+1, y, z$.
(iv) $x-1, y, z$.

Molecular modeling

All the modeling studies were carried out on a desktop PC, Intel® Core™ 2 Duo CPU E8200 @ 2.66 GHz, RAM 4 GB operating under Windows 7 professional. It consists of several steps. First, the 3D crystal structures of MurB with PDB code 2Q85 was downloaded from Brookhaven protein data bank (PDB; http://www.rcsb.org/pdb) loaded to Molegro Virtual Docker (MVD 2013.6.0.0 [win32]) program fully functional free trial version with time limiting license [18,19]. All the atom types, charges and bond hybridization were carefully checked. The MolDock Score [GRID] and MolDock Optimizer routines as implemented in Molegro Virtual Docker (MVD version 2013.6.0.0). The non-bonded oxygen atoms of waters, present in the crystal structure were removed. ChemBio3D Ultra 10^5 was used to draw the 3D structures of different ligands. Ligands were further pre-optimized using free version of Marvinsketch 4.1.13 from Chemaxon Ltd [6] with MM force field and saved in Tripos mol2 file format. MolDock score functions were used with a 0.3 Å grid resolution. Prior to the calculations of the subject compounds, the MVD software was benchmarked docking the naphthyl tetronic acid inhibitor.

Results and discussion

Chemistry

The synthetic strategies adopted to obtain the target compounds are depicted in Scheme 1. The 2-thioxothiazolidin-4-one derivatives were synthesized by the literature procedure described by Barakat et al. [7]. 2-Thioxothiazolidin-4-one derivatives were prepared by condensing the 2-thioxothiazolidin-4-one with

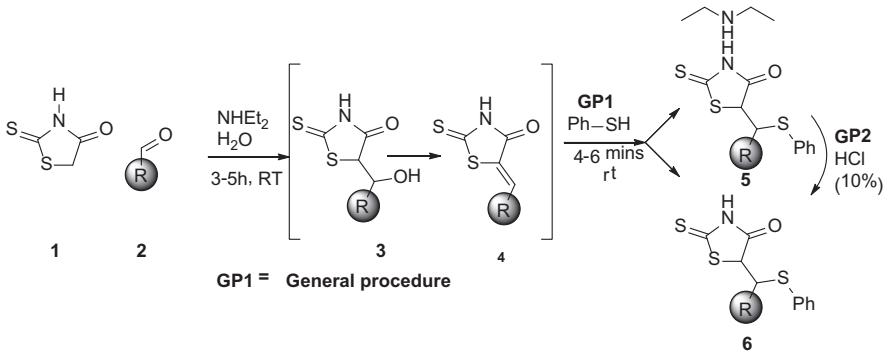

Scheme 1. Synthesis of 2-thioxothiazolidin-4-one derivatives by Aldol-thia-Michael reaction in aqueous diethylamine.

various aldehyde in the presence of aqueous diethylamine medium to yield the Aldol products with subsequently addition of thiol to obtain thia-Michael adducts. The three-component one pot aqueous diethylamine-promoted synthesis of these target molecules provides an environment friendly and benign synthesis with rapid and easy access to 2-thioxothiazolidin-4-one compounds in good to excellent yields.

The structure of **3** (Fig. 2) was confirmed by X-ray crystal structure analysis. CCDC-989933 contains the supplementary crystallographic data for this compound. These data can be obtained free of charge from the Cambridge Crystallographic Data Centre via www.ccdc.cam.ac.uk/data_request/cif.

A clear intense yellow block-like specimen of $C_{10}H_7Cl_2NO_2S_2{\cdot}H_2O$, approximate dimensions 0.301 mm × 0.420 mm × 0.580 mm, was used for the X-ray crystallographic analysis. A total of 630 frames were collected by Bruker APEX-II D8 Venture. The frames were integrated with the Bruker SAINT software package using a narrow-frame algorithm [20,21] The integration of the data using a triclinic unit cell yielded a total of 54109 reflections to a maximum θ angle of 30.71° (0.70 Å resolution), of which 8093 were independent (average redundancy 6.686, completeness = 98.8%, R_{int} = 7.05%, R_{sig} = 4.84%) and 6001 (74.15%) were greater than $2\sigma(F^2)$. The final cell constants of a = 9.0528(11) Å, b = 10.6637(13) Å, c = 14.8063(18) Å, α = 85.702(4)°, β = 75.933(4)°,

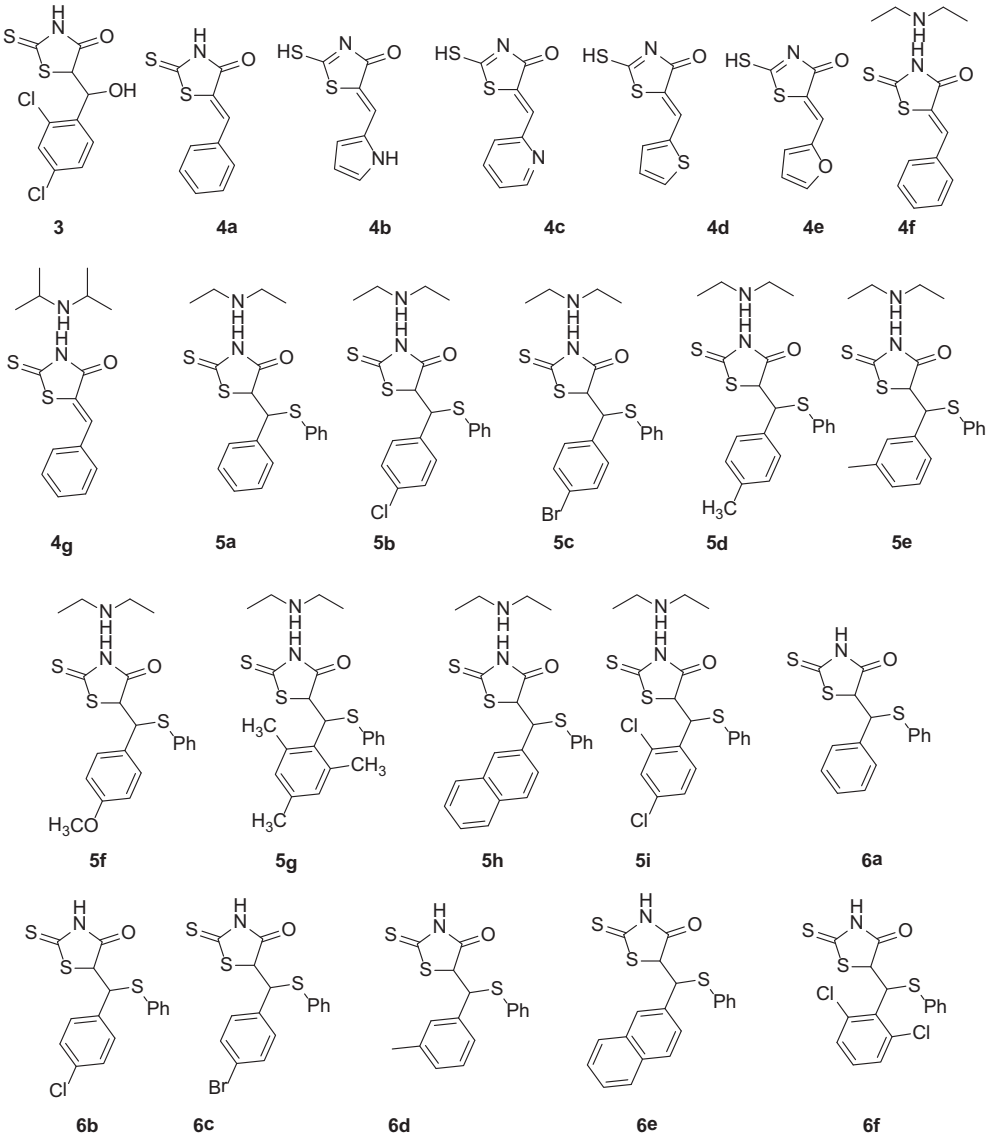

The structures of these compounds were characterized by ^{1}H NMR, ^{13}C NMR, MS, IR, elemental analysis, and X-ray diffraction crystallography in a similar manner as those earlier compounds that have been fully reported by our group [7].

Single crystal X-ray diffraction analysis of compound of ***3***

Interestingly, the Aldol intermediate **3** can be separated by stopping the reaction after 0.5 h and the product was unambiguously elucidated by X-ray diffraction analysis.

γ = 72.013(4)°, volume = 1318.7(3) Å^3, are based upon the refinement of the XYZ-centroids of 9768 reflections above 20 $\sigma(I)$ with 4.863° < 2θ < 61.11°. Data were corrected for absorption effects using the multi-scan method (SADABS). The ratio of minimum to maximum apparent transmission was 0.872. The calculated minimum and maximum transmission coefficients (based on crystal size) are 0.6520 and 0.7930.

The final anisotropic full-matrix least-squares refinement on F^2 with 357 variables converged at $R1$ = 4.72%, for the observed data and $wR2$ = 12.59% for all data. The goodness-of-fit was 1.021. The largest peak in the final difference electron density synthesis was 0.843 e$^-$/Å^3 and the largest hole was −0.398 e$^-$/Å^3 with an RMS deviation of 0.117 e$^-$/Å^3. On the basis of the final model, the calculated density was 1.643 g/cm^3 and F(000), 664 e$^-$.

The asymmetric unit contains two molecules of the compound and two water molecules with disorder in the hydrogen atoms (Fig. 2). The molecular structure of compound **3** is composed of a thiazole ring (S1/C1/N1/C2–C3) which is linked to a phenyl ring (C5–C10) through C4. The thiazole ring forms a dihedral angle of 41.88 (3)° with the adjacent benzene ring. The molecule is bent (Fig. 2) at the C4 atom with a S1A–C3A–C4A–C5A torsion angle of −58.1 (2)° and S1B–C3B–C4B–C5B torsion angle of −63.9 (2)°. In the crystal structure intermolecular O–H···O and N–H···O hydrogen bonds are observed (Fig. 3 and Table 1).

Computational details

All the quantum chemical calculations of the $C_{10}H_7Cl_2NO_2S_2$, **3a** and its H-bonded complex $C_{10}H_7Cl_2NO_2S_2{\cdot}H_2O$, **3b** were performed by applying DFT method with the B3LYP functional and 6-311G(d,p) basis set using Gaussian 03 software [22]. The input files were taken from the CIF file obtained from our reported X-ray single crystal measurements. The geometries were optimized by minimizing the energies with respect to all the geometrical parameters without imposing any molecular symmetry constraints. GaussView4.1 has been used to draw the structures of the optimized geometries [23]. Frequency calculations at the optimized geometry were done to confirm the optimized structures to be an energy minimum. The true energy minimum at the optimized geometry of the studied compounds was confirmed by absence of any imaginary frequency modes. The possible electronic transitions of **3b** were calculated by the TD-DFT method. The natural bond orbital analyses were performed using the NBO calculations as implemented in the Gaussian 03 package [24] at the DFT/B3LYP level.

Molecular geometry

The optimized bond lengths and bond angles obtained for the studied compounds using the B3LYP method with 6-311G(d,p)

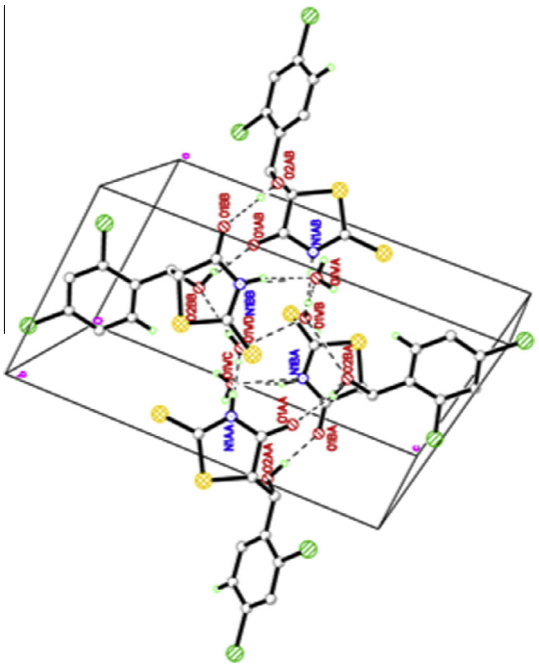

Fig. 3. Crystal packing showing intermolecular O–H···O and N–H···O hydrogen bonds as dashed lines.

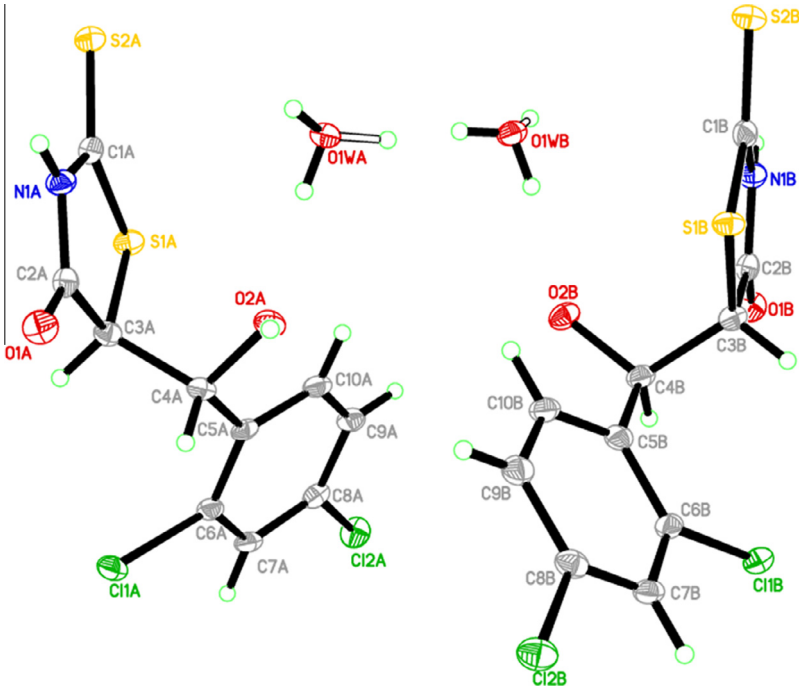

Fig. 2. ORTEP diagram of the structure of **3**.

basis set are given in Table 2; while the atom numbering of the optimized structures are given in Fig. 4. Both molecules possesses C_1 point group. The optimized geometry of **3b** is compared with the structural parameters obtained from the CIF file. Generally, the bond lengths and bond angles are predicted very well. Most of bond lengths are overestimated except C5–O9 bond. The maximum deviations of the calculated bond length and bond angle values from the experimental data are 0.028 Å (C10–S1) and 2.416° (C12–C10–S1) respectively. These deviations are attributed to the phase difference between the calculations and the experiment. The calculations refer to an isolated molecule in the gas phase, while the experimental data are those for the molecule in the solid phase. The experimental values of C–C–C angles for benzene ring are around the typical hexagonal angle of 120° [25]. The calculated C–C–C bond angles values are in the range of 118.54–122.27° (exp. 118.25–122.37°). A comparison between the calculated geometric parameters of **3a** and **3b** is shown in Fig. 5 and Table 2. The effect of H-bonding interactions between **3a** and water molecule seems to be insignificant. There is small increase for the C12–O6 bond length due to H-bonding interactions with the water molecule. The rest of the geometric parameters are affected very little.

Natural atomic charges

The natural atomic charges (NAC) at the different atomic sites of **3a** and **3b** calculated using the DFT/B3LYP method are collected in Table 3. All the hydrogen atoms are electropositive. For **3a**, the most positive H-sites are H23 (+0.4290) and H24 (+0.4739). In contrast, the C-atoms have negative charge densities except C9, C12 and C15. The most positive C-site is C12 as it lies between the two strong electronegative O and N atoms. Similar observations are obtained for **3b**. Moreover, the O6 and O25 have the highest

Table 2
Comparative experimental and calculated bond distances (Å) and bond angles (°) of the studied compound.

Parameter[a]	DFT		X-ray	Parameter[a]	DFT		X-ray
	3a	**3b**			**3a**	**3b**	
R(1–8)	1.764	1.766	1.747	A(3–15–16)	117.22	117.06	117.99
R(1–10)	1.842	1.843	1.815	A(4–18–16)	119.09	119.07	118.85
R(2–8)	1.640	1.637	1.627	A(4–18–19)	119.81	119.89	119.23
R(3–15)	1.765	1.765	1.750	A(5–9–7)	124.66	124.86	125.39
R(4–18)	1.754	1.754	1.744	A(5–9–10)	124.56	124.47	122.71
R(5–9)	1.208	1.209	1.222	A(12–6–24)	107.79	107.19	104.89
R(6–12)	1.418	1.427	1.425	A(6–12–10)	110.52	110.74	109.59
R(6–24)	0.963	0.964	0.813	A(6–12–13)	110.38	108.96	108.53
R(7–8)	1.379	1.382	1.374	A(6–12–14)	109.08	110.07	109.85
R(7–9)	1.382	1.380	1.354	A(8–7–9)	119.81	119.71	118.77
R(7–23)	1.013	1.013	0.827	A(8–7–23)	119.62	119.54	120.52
R(9–10)	1.527	1.528	1.513	A(9–7–23)	120.28	120.38	120.55
R(10–11)	1.092	1.093	0.979	A(7–9–10)	110.76	110.66	111.88
R(10–12)	1.553	1.549	1.545	A(9–10–11)	108.07	107.90	109.29
R(12–13)	1.095	1.094	0.980	A(9–10–12)	109.61	110.02	109.06
R(12–14)	1.516	1.515	1.506	A(11–10–12)	109.19	108.59	109.29
R(14–15)	1.398	1.400	1.401	A(10–12–13)	105.37	105.42	108.47
R(14–21)	1.398	1.399	1.392	A(10–12–14)	112.37	112.57	111.84
R(15–16)	1.391	1.390	1.383	A(13–12–14)	109.07	108.92	108.49
R(16–17)	1.081	1.081	0.929	A(12–14–15)	122.66	121.60	121.53
R(16–18)	1.389	1.389	1.378	A(12–14–21)	119.99	121.03	121.57
R(18–19)	1.390	1.389	1.388	A(15–14–21)	117.35	117.37	116.89
R(19–20)	1.082	1.082	0.931	A(14–15–16)	122.19	122.27	122.37
R(19–21)	1.390	1.390	1.384	A(14–21–19)	121.74	121.50	122.31
R(21–22)	1.081	1.083	0.930	A(14–21–22)	118.19	119.69	118.84
A(8–1–10)	93.31	93.09	93.10	A(15–16–17)	120.48	120.47	120.89
A(1–8–2)	125.09	125.15	124.79	A(15–16–18)	118.57	118.54	118.25
A(1–8–7)	109.62	109.59	110.15	A(17–16–18)	120.95	120.99	120.86
A(1–10–9)	106.06	106.00	106.10	A(16–18–19)	121.10	121.04	121.92
A(1–10–11)	108.18	107.95	109.33	A(18–19–20)	120.26	120.35	120.83
A(1–10–12)	115.48	116.09	113.67	A(18–19–21)	119.05	119.29	118.24
A(2–8–7)	125.29	125.26	125.06	A(20–19–21)	120.69	120.36	120.93
A(3–15–14)	120.58	120.67	119.64	A(19–21–22)	120.07	118.81	118.85

[a] Atom numbering referred to Fig. 4.

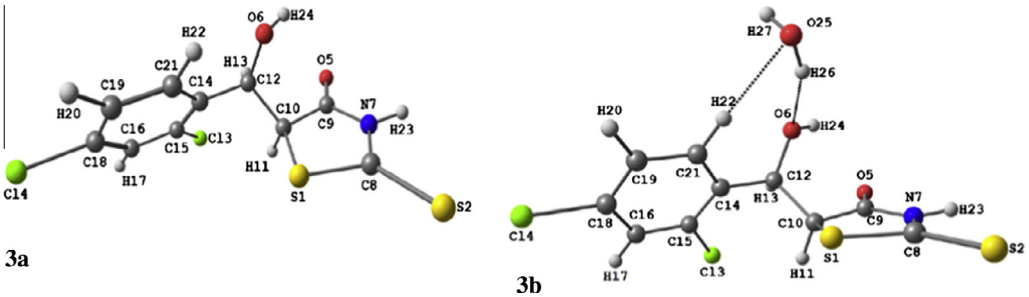

Fig. 4. The optimized molecular structures of the studied compounds **3a,b**.

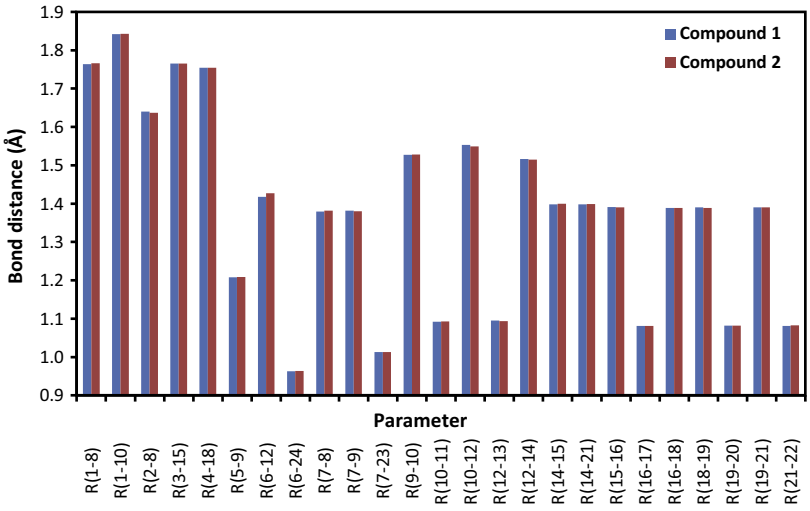

Fig. 5. Comparison between the calculated bond distances of **3a** and **3b**.

Table 3
The calculated natural atomic charge values of the studied molecules.

Atom	3a	3b
S1	0.3379	0.3413
S2	−0.0466	−0.0312
Cl3	−0.0065	−0.0071
Cl4	0.0079	0.0095
O5	−0.5778	−0.5830
O6[a]	**−0.7419**	**−0.7665**
N7	−0.6213	−0.6211
C8	−0.1183	−0.1229
C9	0.7091	0.7082
C10	−0.4223	−0.4233
H11	0.2527	0.2537
C12	0.1361	0.1380
H13	0.2107	0.2139
C14	−0.0975	−0.1033
C15	0.0054	0.0069
C16	−0.2527	−0.2534
H17	0.2369	0.2372
C18	−0.0015	−0.0003
C19	−0.2199	−0.2173
H20	0.2248	0.2267
C21	−0.1561	−0.1648
H22	0.2379	0.2433
H23	0.4290	0.4300
H24	0.4739	0.4817
O25		−0.9064
H26		0.4681
H27		0.4423

[a] Largest NAC variation.

negative charge density for **3a** and **3b** respectively. The NAC values at all atomic sites are affected very little due to the interaction between **3a** and the water molecule. The largest variation of the NAC values due to H-bonding interaction with the water molecule occurs at O6. The negative charge density at this atomic site is increased from −0.7419 in case of **3a** to −0.7665 for **3b**.

Molecular electrostatic potential (MEP)

The molecular electrostatic potential (MEP) is a useful property for predicting sites and relative reactivities towards electrophilic and nucleophilic attack and in the studies of hydrogen bonding interactions [26,27]. The MEP of **3a** and **3b** calculated using B3LYP with 6-311G(d,p) basis set is used to predict the reactive sites for electrophilic and nucleophilic attack. The negative (red) regions of the MEP are related to electrophilic reactivity and the positive (blue) regions to nucleophilic reactivity, as shown in Fig. 6. It can be seen from this figure that, negative regions are mainly localized over the O5 and O25 atoms. These sites present the most reactive sites for electrophilic attack and are the most H-acceptor sites for making H-bonding interactions. The maximum positive regions are localized on the H23, H24, H25 and H27 atoms which represent the most reactive sites for nucleophilic attack as well as for being the H-donor sites for the H-bonding interactions. These results agree with our reported X-ray structure of the studied compound.

Electronic absorption spectra and frontier molecular orbitals (FMOs)

The frontier molecular orbitals can offer a reasonable qualitative indication on the excitation properties and the ability of the molecule towards electron transport process [28,29]. The HOMO and LUMO energies of **3b** were investigated using the DFT/B3LYP method. Fig. 7 shows the isodensity surface plots of HOMO and LUMO. It can be seen from Fig. 7 that the electron densities of HOMO and LUMO are mainly localized on the thiazole ring. The E_{HOMO}, E_{LUMO} and transition energies (ΔE) for **3b** are calculated to be −6.8097 eV, −2.4324 eV and 4.37726 eV respectively. In order to understand the accurate electronic transitions of the titled compound, **3b**, the first twenty spin allowed singlet–singlet excitations were calculated using TD-DFT. The results are shown in Table 4 which represents the calculated λ_{max} values and the oscillator strength (f) of these transition bands with their major contributions of molecular orbitals. Of these electronic transitions obtained from the current calculations, the most intense transition band is calculated at 283.9 nm corresponds to the electronic transitions from the HOMO-2/HOMO-1 to LUMO.

Natural bond orbital (NBO) analysis

A useful aspect of the NBO method is that it gives information about the intra- and intermolecular interactions. Delocalization of electron density between occupied Lewis-type (bond or lone pair) NBO orbitals and formally unoccupied NBO orbitals correspond to a stabilizing donor–acceptor interaction. The larger the interaction energies ($E^{(2)}$) value, the more intensive is the interaction between electron donors and electron acceptors, i.e. the more

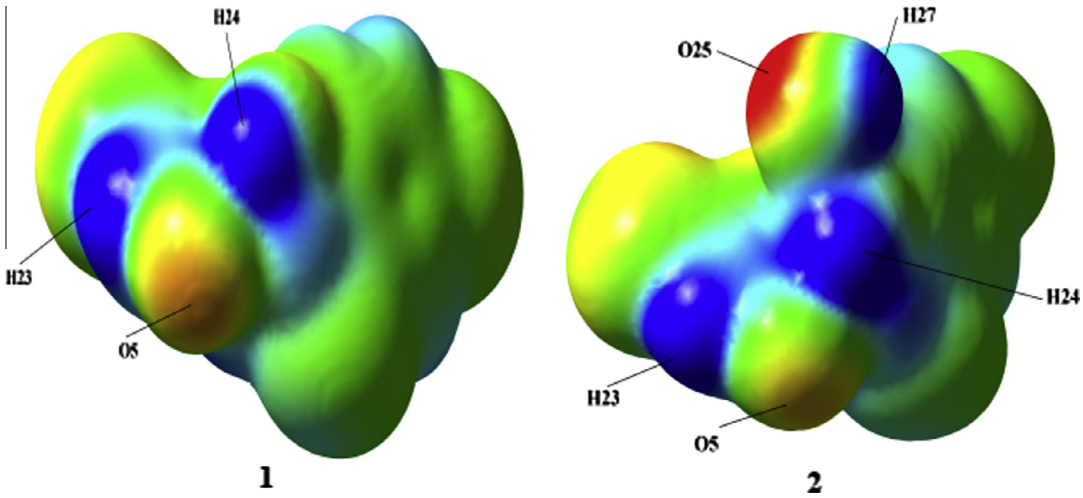

Fig. 6. Molecular electrostatic potentials (MEP) mapped on the electron density surface calculated by the DFT/B3LYP method.

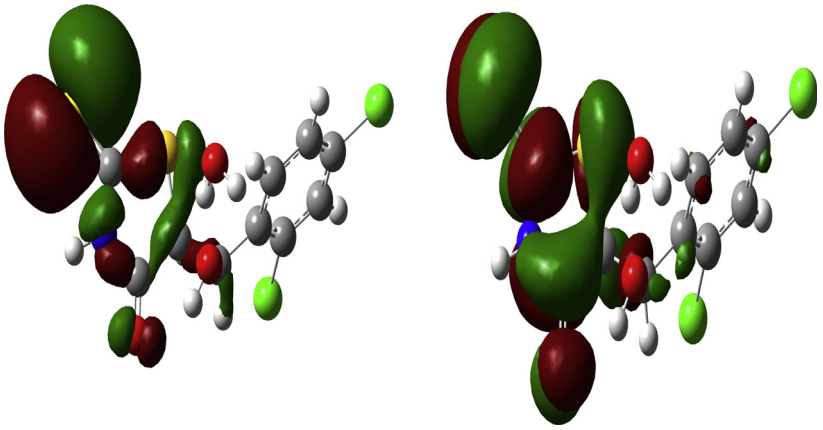

Fig. 7. The ground state isodensity surface plots for the frontier molecular of **3b.**

Table 4
The calculated electronic spectra of **3b** using the TD-DFT method.

λ_{max}	f_{osc}	Major contribution	λ_{max}	f_{osc}	Major contribution
394.3	0.0003	H → L (93%)	236.6	0.0056	H-4 → L (89%)
283.9	0.2024	H-2 → L (15%), H-1 → L (68%)	231.1	0.0054	H-2 → L+2 (15%), H-1 → L+2 (76%)
277.3	0.0335	H-2 → L (77%)	229.7	0.0267	H-5 → L (11%), H → L+3 (65%)
257.8	0.0084	H-3 → L (90%)	226.3	0.0322	H → L+4 (50%), H → L+5 (35%)
256.9	0.0032	H → L+1 (77%), H → L+3 (10%)	225.0	0.0185	H-1 → L+1 (15%), H-1 → L+3 (47%), H-1 → L+5 (14%)
248.7	0.0115	H-6 → L (73%)	221.9	0.1243	H-3 → L+2 (11%), H-2 → L+1 (61%)
245.7	0.0013	H-3 → L+1 (17%), H-2 → L+2 (22%), H → L+2 (36%)	212.8	0.0144	H-2 → L+4 (13%), H-1 → L+3 (14%), H-1 → L+4 (48%)
243.4	0.0085	H-2 → L+2 (12%), H-1 → L+1 (10%), H → L+2 (61%)	212.2	0.0025	H-2 → L+4 (40%), H-1 → L+3 (13%), H-1 → L+5 (22%)
242.2	0.0055	H-1 → L+1 (59%)	210.5	0.0005	H-8 → L (38%), H-7 → L (56%)
237.8	0.1168	H-5 → L (53%), H → L+3 (14%)	207.7	0.0046	H → L+4 (40%), H → L+5 (50%)

donating tendency from electron donors to electron acceptors and the greater the extent of conjugation of the whole system [30].

NBO analysis has been performed on the studied molecules at the B3LYP/6-311G(d,p) level in order to elucidate the delocalization of electron density within the molecule. The energy of these interactions ($E^{(2)}$) can be estimated by the second-order perturbation theory [31]. The stabilization energies ($E^{(2)}$) obtained from the second order perturbation theory for compounds **3a**and **3b** are reported in Table 5. The intramolecular charge transfer (ICT) interaction is formed by the orbital overlap between π(C C) and π* (C–C) bond orbitals causing stabilization of the system up to 96.34 kJ/mol. The most important interaction energy in the studied molecules, is electron donating from LP(1)N7 to the antibonding π*(S2–C8) and π*(O5–C9) NBOs resulting in maximum stabilization up to 263.89 kJ/mol. The LP(1)O6 → σ*(O25–H26) and LP(2)O25 → σ*(C21–H22) intramolecular charge transfer interactions clearly manifests the evidences of the intramolecular H-bonding interactions. The interaction energies ($E^{(2)}$) due to these

Table 5
The stabilization energies $E^{(2)}$ (kJ/mol) of the most important charge transfer interactions in the studied compounds using B3LYP method.

Donor NBO (*i*)	Acceptor NBO (*j*)	$E^{(2)}$ kJ/mol **3a**	$E^{(2)}$ kJ/mol **3b**
π(C14–C15)	π*(C16–C18)	85.41	84.24
π(C14–C15)	π*(C19–C21)	77.12	76.83
π(C16–C18)	π*(C14–C15)	80.76	82.31
π(C16–C18)	π*(C19–C21)	77.71	77.37
π(C19–C21)	π*(C14–C15)	91.10	91.57
π(C19–C21)	π*(C16–C18)	95.04	96.34
LP(2)S1	π*(S2–C8)	166.89	161.69
LP(2)S2	σ*(S1–C8)	64.94	65.82
LP(2)S2	σ*(N7–C8)	57.40	58.20
LP(3)Cl3	π*(C14–C15)	51.08	51.25
LP(3)Cl4	π*(C16–C18)	54.14	54.47
LP(2)O5	σ*(N7–C9)	113.59	112.50
LP(2)O5	σ*(C9–C10)	89.97	89.72
LP(2)O6	σ*(C10–C12)	38.81	32.74
LP(1)N7	π*(S2–C8)	263.98	255.48
LP(1)N7	π*(O5–C9)	195.86	190.54
LP(1)O6	σ*(O25–H26)		16.08
LP(2)O25	σ*(C21–H22)		10.38

ICT were calculated to be 10.38 and 16.08 kJ/mol respectively. The stronger O–H···O H-bonds further stabilizes the system more than the weaker C–H···O interactions.

Antimicrobial assay

Anti-bacterial activity studies

The antimicrobial activity and the Minimum Inhibitory Concentration (MIC) were performed by cup plate method and microbroth dilution method respectively with different strains [15–17].

The prepared compounds were screened for their antibacterial activity against Gram-positive bacteria (*S. aureus* ATCC 29213, *B. subtilis* ATCC 10400 and *E. faecalis* ATCC 2912) and Gram-negative bacteria (*Pseudomonas aeruginosa* ATCC 27853, *Proteus vulgaris* ATCC 6380, *Klebsiella pneumoniae* ATCC 27736, and *Escherichia coli* ATCC 25218). Briefly, 50 μL of 2× Mueller–Hinton broth (Oxoid Chemical Co. UK) was dispensed into wells of sterile 96 microtitre plate. A 50 μL of the tested compounds (512 mg/μL) was pipetted into the wells in first well and mixed the contents by using multi-pippetor by pipetting up and down 6–8 times. Then 50 μL from the first column was withdrawn and added to the second well to make a twofold dilution. This procedure was repeated down to 12th well to reach the concentration of 0.25 μg/mL. A 50 μL was discarding from 12th well. The tested organisms were grown to mid-log phase in Mueller–Hinton broth to the right A560 and diluted 100-fold in the same medium to obtain 1×10^5–1×10^6 CFU/mL. Ciprofloxacin wasused as positive controls for bacteria. A 100 μL of bacterial inoculums (1×10^5–1×10^6 CFU/mL) was dispensed into wells to give final bacterial inocula was 0.5×10^5–0.5×10^6 CFU/mL. The microtiter plates were incubated at 35 °C for 18 h. After the incubation period, the results of MIC were recorded manually and interpreted according to the recommendations of EUCAST. The MIC (expressed in μg/mL) was the lowest concentration of the test substance that completely inhibited growth of the microorganism. The results of antibacterial activity of the compounds are summarized in Table 6. The tested compounds were specifically active against Gram-positive bacteria (*Staphylococcus auerus*, *B. subtilis*, and *E. faecalis*). All examined derivatives were inactive against Gram-negative rods (data not shown).

Compounds **3**, **4a,e,g,f**, **5a,b,d,e,g,h,I** and **6b–f** possessed good activity against tested Gram-positive *S. auerus*, in comparison with the reference compound Ciprofloxacin. For most bacterial strains

Table 6
Antimicrobial activity of 2-thioxothiazolidin-4-one derivatives (**3**–**6**).

#	Comp. No.	Gram-positive bacteria						Fungi	
		Staphylococcus aureus ATCC 29213 (COCCI)		*Bacillus subtilis* ATCC 10400 (BACILI)		*Enterococcus faecalis* ATCC2912 (COCCI)		*Candida albicans* ATCC2091	
		Sensitivity	**MIC**	Sensitivity	**MIC**	Sensitivity	**MIC**	Sensitivity	**MIC**
1.	3	++	**64**	++	**64**	+	**128**	++	**64**
2.	4a	+++	**32**	++++	**16**	+	**128**	++	**64**
3.	4b	N.A.	ND	N.A.	ND	N.A.	ND	+	ND
4.	4c	++	**64**	+	**128**	++	**64**	+++	**32**
5.	4d	+	ND	N.A.	ND	+	ND	+	ND
6.	4e	++	**64**	++++	**16**	++	**64**	++	**64**
7.	4g	+++	**32**	++++	**16**	+	**128**	++	**64**
8.	4f	+++	**32**	+++	**32**	++	**64**	+++	**32**
9.	5a	+++	**32**	+++	**32**	+	**128**	++	**64**
10.	5b	+++	**32**	++++	**16**	+	**128**	+++	**32**
11.	5c	+	ND	+	ND	+	ND	+	ND
12.	5d	+++	**32**	++	**64**	+	**128**	++	**64**
13.	5e	+++	**32**	++++	**16**	++	**64**	+++	**32**
14.	5f	N.A.	ND	+	ND	+	ND	+	ND
15.	5g	++	**64**	++++	**16**	+	**128**	+++	**32**
16.	5h	++	**64**	++++	**16**	++	**64**	+++	**32**
17.	5i	+++	**32**	++++	**16**	+	**128**	+++	**32**
18.	6a	+	**128**	++	**64**	++	**64**	++	**64**
19.	6b	++	**64**	++	**64**	++	**64**	+++	**32**
20.	6c	++	**64**	+++	**32**	++	**64**	+++	**32**
21.	6d	++	**64**	+++	**32**	+	**128**	+++	**32**
22.	6e	++	**64**	+++	**32**	++	**64**	++	**64**
23.	6f	++	**64**	++++	**16**	++	**64**	++	**64**
24	**CI**	++++	**0.5**	++++	**0.25**	++++	**0.125**		ND
25	**IT**		ND		ND		ND	++++	**0.5**

[a] Antimicrobial activities were expressed as inhibition diameter zones in millimeters (mm) as follows: N.A. (no activity) <4 mm; + (weak) = 5–9 mm; ++ (moderate) = 10–15 mm; +++ (strong) = 16–20 mm and ++++ (very strong) ⩾21 mm. The experiment was carried out in triplicate and the average zone of inhibition was calculated. MIC = Minimum Inhibitory Concentration; MIC expressed in μg/mL; MIC was done by microbroth dilution method according to EUCAST; CI = Ciprofloxacin; IT = Itraconazole and ND: Not Determine.

tested the MIC values of compounds **3, 4a,e,g,f**, **5a,b,d,e,g,h,l** and **6b–f** were between 32 and 64 μg/mL.

All compounds **3, 4a,c,e,g, 5a,b,d,e,** and **6a–f** showed MIC values in the range of 16–128 μg/mL against *B. subtilis* bacteria and *E. faecalis* (Table 6). Graphical representation of MIC (μg/mL) of compounds (**3–6**) against bacterial strains (Fig. 8).

The results of antibacterial activity (Table 6) revealed that among all compounds, **4a,e**, **5a,e,g–i** and **6f** were found to be most active against Gram-positive bacteria MIC value of 16 μg/mL with diameter of growth of inhibition zone of ⩾21 mm.

In vitro antifungal activity

Antifungal activity of all compounds (**3–6**) was evaluated by selecting one yeast strain *C. albicans* ATCC 2091 on the basis of their clinical importance and MIC was determined [17]. The diameter of growth of inhibition zone (mm) and MIC (μg/mL) of all compounds was determined using itraconazole as a standard drug. The results of antifungal activity of all compounds (**3–6**) are shown in Table 6. It can be seen from Table 6 that all compounds showed good antifungal activity. The diameter of growth of inhibition zone was observed in the range of 5–20 mm and MIC in the range of 32–64 μg/mL for yeast *C. albicans* ATCC 2091 for compounds **3–6**.

Molecular modeling study

Molecular docking is a very popular method employed to investigate drug interactions. Docking-based drug design by the use of structural biology remains one of the most logical and esthetically pleasing approaches in the drug discovery process. MurB enzyme is essential for peptidoglycan biosynthesis in the bacterial cell wall. The absence of a homologue in eukaryotic cells makes MurB a good target for small molecule inhibitors with the potential to have antibacterial activity. Biochemical characterization and X-ray structural analysis of MurB from *E. coli* were studied before and based on a cocrystal structure study of *E. coli* MurB with naphthyl tetronic acid inhibitor (PDB code 2Q85) it was found that the cocrystallized inhibitor interacts with residues Leu218, Asn233, Pro252, Tyr254 and Ala264. On other hand, for the carboxylate group of uridine diphosphate *N*-acetylglucosamine, the normal substrate of the enzyme interacts with residues Arg159 and Glu325, whereas the diphosphate moiety of the substrate interacts with residues Tyr190, Lys217, Asn233, and Glu288 [32,33].

To compare the binding affinity of the newly synthesized compounds, they were docked in the empty binding site of MurB (PDB entry 2Q85).The naphthyl tetronic acid (standard inhibitor) reveals MolDock score of −113 and forms two hydrogen bonds between its hydroxyl groups on the furan ring with Gln288 and Asn233 with a bond distance of 2.90 and 3.32 Å, respectively (Fig. 9). Compounds **5a–i** and **6a–f** exhibited MolDock scores rangingfrom −122 to −103, compared to compounds **3** and **4a–f** which have bad MolDock sores ranging from −87 to −80. Compounds **5h**, **5f** and **6e** have highest MolDock scores in this study; −122, −117 and −116 respectively. Compound **5h** forms two hydrogen bonds between the oxygen of thiazolidone ring with the guanido group of Arg214 of distances 2.96 and 3.22 Å. The naphthyl moiety was also located in the hydrophobic pocket in the active site (Fig. 9). Lipophilicity appears to play crucial role in **5h** inhibitory activity, as naphthyl moiety is properly oriented to the more lipophilic area of the MurB binding site through formation of CH-π interactions [34,35].

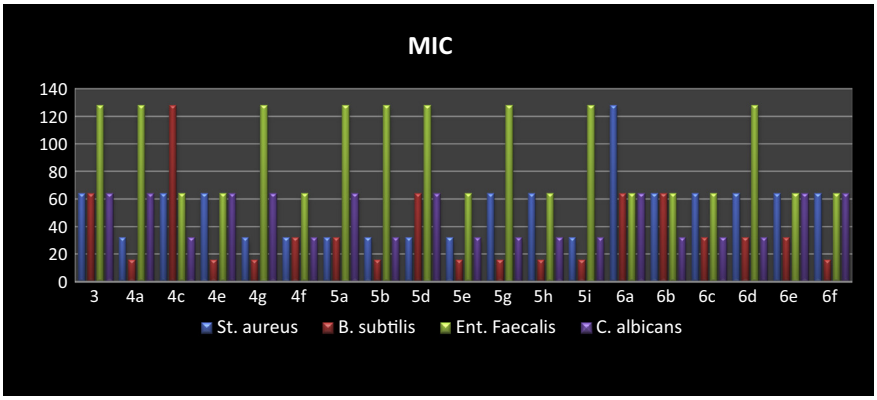

Fig. 8. Graphical representation of MIC (μg/mL) of compounds (**3–6**) against bacterial strains.

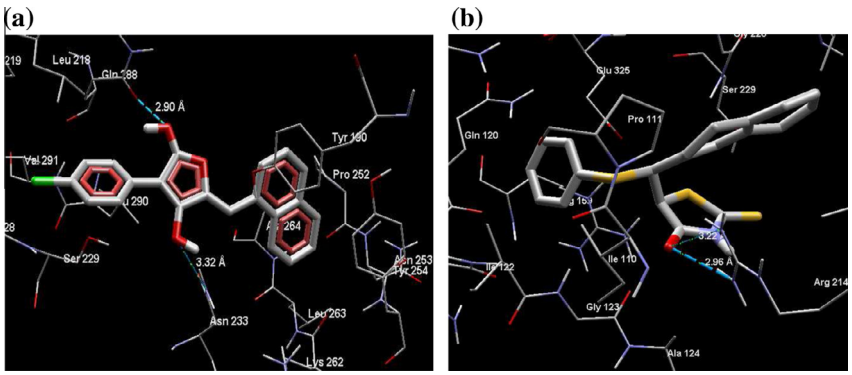

Fig. 9. (a) Best pose of the naphthyl tetronic acid (Sticks) with hydrogen bonding to MurB active site. (b) Interactions between compound **5h** (Sticks) with an MurB active site. Blue dashes represent H-bonds. (For interpretation of the references to colour in this figure legend, the reader is referred to the web version of this article.)

Conclusions

In conclusion, 4-thiazolidinone derivatives were prepared and studied for antimicrobial activity. The DFT calculations showed that, the interaction between **3** and water molecule has very little effect on its geometric parameters. Only a slight elongation for the C12–O6 bond has been predicted. The natural atomic charge density at O6 is shifted to more negative value due to the H-bonding interaction with the water molecule. MEP map showed that O5 and O25 atoms are the most reactive sites for electrophilic attack while the H23, H24, H25 and H27 are the most reactive sites for nucleophilic attack. The NBO calculations showed that, the O–H···O and C–H···O H-bonding interactions stabilized the system up to 16.08 kJ/mol. Most of the studies have demonstrated the efficacy of antimicrobial agent in a particular Gram-positive bacteria. All compounds showed good antifungal activity. The docking studies of compound 5 h at the MurB binding site were also performed.

Author contributions

Hany Al-Najjar: Carried out the experimental part; Mohamed Al-Agamy carried out the antimicrobial activity; H. Ghabbour and H.-K. Fun carried out the X-ray part; Saied M. Soliman performed the computational studies; Y. Mabkhot, and A. Al-Majid: helped in the results and discussion and writing the manuscript; A. Barakat: proposed the subject, and designed the study. All the authors read and approved the final manuscript.

Acknowledgments

The authors extend their appreciation to the Deanship of Scientific Research at King Saud University for funding the work through the research group project Number RGP- VPP- 257.

References

[1] R. Jeyaraman, S. Avila, Chem. Rev. 81 (1981) 149–174.
[2] A.K. Jain, A. Vaidya, V. Ravichandran, S.K. Kashaw, R.K. Agrawal, Bioorg. Med. Chem. 20 (2012) 3378–3395.
[3] W.S. Hamama, M.A. Ismail, S. Shaaban, H.H. Zoorob, J. Heterocycl. Chem. 45 (2008) 939–1253.
[4] A. Verma, S.K. Saraf, Eur. J. Med. Chem. 43 (2008) 897–905.
[5] R.M. Abdel-Rahman, Boll. Chim. Farm. 140 (2001) 401–410.
[6] S.P. Singh, S.S. Parmar, K. Raman, V.I. Stenberg, Chem. Rev. 81 (1981) 175–203.
[7] A. Barakat, A.M. Al-Majid, H.J. Al-Najjar, Y.N. Mabkhot, H.A. Ghabbour, H-K. Fun, RSC Adv 4 (2014) 4909–4916.
[8] H.J. Al-Najjar, A. Barakat, A.M. Al-Majid, Y.N. Mabkhot, M. Weber, H.A. Ghabbour, H.-K. Fun, Molecules 19 (2014) 1150–1162.
[9] A. Barakat, A.M.A. Al Majid, M.S. Islam, Z.A. Al-Othman, Tetrahedron 69 (2013) 5185–5192.
[10] D. Kini, M. Ghate, Eur. J. Chem. 8 (2011) 386–390.
[11] R. Maccari, A.D. Corso, M. Giglio, R. Moschini, U. Mura, R. Ottana, Bioorg. Med. Chem. Lett. 21 (2011) 200–203.
[12] A. Ottana, R. Maccari, M. Giglio, A.D. Corso, M. Cappiello, U. Mura, S. Cosconati, M. Marinelli, E. Novellino, S. Sartini, C. La-Motta, F.D. Settimo, Eur. J. Med. Chem. 46 (2011) 2797–2806.
[13] C.J. Anders, J.J. Bronson, S.V. D'Andrea, S.M. Deshpande, P.J. Falk, K.A. Grant-Young, W.E. Harte, H. Ho, P.F. Misco, J.G. Robertson, D. Stock, Y. Sun, A.W. Walsh, Bioorg. Med. Chem. Lett. 10 (2000) 715–717.
[14] M. Schreiber, J. Res. A. Matter Curr. Opin. Cell Biol. 21 (2009) 325–340.
[15] A. Barakat, A.M. Al-Majid, F.M. Al Qahatany, M.S. Islam, M.H.M. Al-Agamy, Bull. Korean Chem. Soc. 35 (2014) 562–568.
[16] A.C. Scott, in: J.G. Collee, J.P. Duguid, A.G. Fraser, B.P. Marmion (Eds.), Laboratory control of antimicrobial therapy, thirteenth ed., Mackie and MacCartney Practical Medical Microbiology, vol. 2, Churchill Livingstone, 1989, pp. 161–181.
[17] The European Committee on Antimicrobial Susceptibility Testing, Antimicrobial Susceptibility Testing, 2014 <http://www.eucast.org>.
[18] T.E. Benson, C.T. Walsh, J.M. Hogle, Biochemistry 36 (1997) 806–811.
[19] T.E. Benson, C.T. Walsh, V. Massey, Biochemistry 36 (1997) 796–805.
[20] G.M. Sheldrick, Acta Crystallogr. A 64 (2008) 112–122.
[21] G.M. Sheldrick, SHELXTL-PC (Version 5.1), Siemens Analytical Instruments Inc., Madison, WI, 1997.
[22] M.J. Frisch et al., Gaussian-03, Revision C.01, Gaussian Inc., Wallingford, CT, 2004.
[23] R. Dennington II, T. Keith, J. Millam, GaussView, Version 4.1, Semichem Inc., Shawnee Mission, KS, 2007.
[24] E.D. Glendening, A.E. Reed, J.E. Carpenter, F. Weinhold, NBO Version 3.1, CI, University of Wisconsin, Madison, 1998.
[25] M. Kurt, S. Yurdakul, J. Mol. Struct. (Theochem) 730 (2005) 59.
[26] J.S. Murray, K. Sen, Molecular Electrostatic Potentials, Concepts and Applications, Elsevier, Amsterdam, 1996.
[27] E. Scrocco, J. Tomasi, Adv. Quantum Chem. 11 (1978) 115.
[28] M. Belletete, J.F. Morin, M. Leclerc, G. Durocher, J. Phys. Chem. A 109 (2005) 6953.
[29] D. Zhenminga, S. Hepinga, L. Yufanga, L. Dianshenga, L. Bob, D. Zhenming, et al., Spectrochim. Acta Part A 78 (2011) 1143.
[30] S. Sebastian, N. Sundaraganesan, Spectrochim. Acta Part A Mol. Biomol. Spectrosc. 75 (2010) 941–952.
[31] I. Hubert Joe, I. Kostova, C. Ravikumar, M. Amalanathan, S.C. Pinzaru, J. Raman Spectrosc. 40 (2009) 1033–1038.
[32] R. Thomsen, M.H. Christensen, J. Med. Chem. 48 (2006) 3315–3321.
[33] Molegro Virtual Docker (MVD 2013.6.0.0), Molegro Bioinformatics Solutions, Danish, 2013 <http://www.molegro.com>.
[34] S.M. Kerwin, Chem.Bio.Office. Ultra, J. Am. Chem. Soc. 132 (2010) (2010) 2466–2469.
[35] Marvinsketch, Version 6.1.0, Chemaxon Company Cheminformatics Technology Products Services, 2013 <http://www.chemaxon.com>.